

## Interaction of O<sup>-</sup> and H<sub>2</sub> at low temperatures

P. Jusko, Š. Roučka, D. Mulin, I. Zymak, R. Plašil, D. Gerlich, M. Čížek, K. Houfek, and J. Glosík

Citation: *The Journal of Chemical Physics* **142**, 014304 (2015); doi: 10.1063/1.4905078

View online: <http://dx.doi.org/10.1063/1.4905078>

View Table of Contents: <http://scitation.aip.org/content/aip/journal/jcp/142/1?ver=pdfcov>

Published by the [AIP Publishing](#)

---

### Articles you may be interested in

[An accurate potential energy surface for the F + H<sub>2</sub> → HF + H reaction by the coupled-cluster method](#)

*J. Chem. Phys.* **142**, 024303 (2015); 10.1063/1.4904546

[Kinetic and dynamic studies of the Cl\(2 P u\) + H<sub>2</sub>O\( X̃ 1 A 1\) → HCl\( X̃ 1 Σ+\) + OH\( X̃ 2 Π\) reaction on an ab initio based full-dimensional global potential energy surface of the ground electronic state of ClH<sub>2</sub>O](#)

*J. Chem. Phys.* **139**, 074302 (2013); 10.1063/1.4817967

[Ultracold collisions of O\(1 D\) and H<sub>2</sub>: The effects of H<sub>2</sub> vibrational excitation on the production of vibrationally and rotationally excited OH](#)

*J. Chem. Phys.* **138**, 164310 (2013); 10.1063/1.4802476

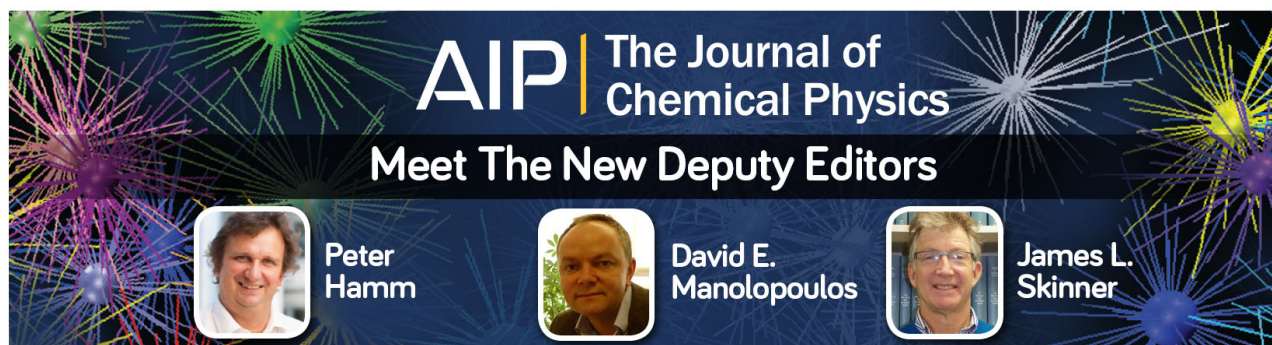
[Nuclear spin dependence of the reaction of H<sub>3</sub><sup>+</sup> with H<sub>2</sub>. I. Kinetics and modeling](#)

*J. Chem. Phys.* **134**, 194310 (2011); 10.1063/1.3587245

[Quantum and classical studies of the O\( 3 P\) + H<sub>2</sub> \(v=0–3, j=0\) → OH + H reaction using benchmark potential surfaces](#)

*J. Chem. Phys.* **120**, 4316 (2004); 10.1063/1.1642580

---



**AIP** | The Journal of  
Chemical Physics

**Meet The New Deputy Editors**

	<b>Peter Hamm</b>		<b>David E. Manolopoulos</b>		<b>James L. Skinner</b>
---	-------------------	---	------------------------------	---	-------------------------

## Interaction of $O^-$ and $H_2$ at low temperatures

P. Jusko,<sup>1</sup> Š. Roučka,<sup>1,a)</sup> D. Mulin,<sup>1</sup> I. Zymak,<sup>1</sup> R. Plašil,<sup>1</sup> D. Gerlich,<sup>1</sup> M. Čížek,<sup>2</sup> K. Houfek,<sup>2</sup> and J. Glosík<sup>1</sup>

<sup>1</sup>Department of Surface and Plasma Science, Faculty of Mathematics and Physics, Charles University in Prague, Prague 180 00, Czech Republic

<sup>2</sup>Institute of Theoretical Physics, Faculty of Mathematics and Physics, Charles University in Prague, Prague 180 00, Czech Republic

(Received 10 September 2014; accepted 15 December 2014; published online 6 January 2015)

Reactive collisions between  $O^-$  and  $H_2$  have been studied experimentally at temperatures ranging from 10 K to 300 K using a cryogenic radiofrequency 22-pole ion trap. The rate coefficients for associative detachment, leading to  $H_2O + e^-$ , increase with decreasing temperature and reach a flat maximum of  $1.8 \times 10^{-9} \text{ cm}^3 \text{ s}^{-1}$  at temperatures between 20 K and 80 K. There, the overall reaction probability is in good agreement with a capture model indicating efficient non-adiabatic couplings between the entrance potential energy surfaces. Classical trajectory calculations on newly calculated potential energy surfaces as well as the topology of the conical intersection seam leading to the neutral surface corroborate this. The formation of  $OH^- + H$  via hydrogen transfer, although occurring with a probability of a few percent only (about  $5 \times 10^{-11} \text{ cm}^3 \text{ s}^{-1}$  at temperatures 10–300 K), indicates that there are reaction paths, where electron detachment is avoided. © 2015 AIP Publishing LLC. [<http://dx.doi.org/10.1063/1.4905078>]

### I. INTRODUCTION

The reaction of  $O^-$  with  $H_2$  is one of the simplest anion-neutral systems and as such it has been studied many times theoretically and experimentally. To our knowledge, there are no measured reaction rate coefficients for temperatures below 170 K. At low temperatures, two exothermic reaction channels are open. These are associative detachment (AD),



and hydrogen atom transfer



with reaction rate coefficients  $k_1$  and  $k_2$ , respectively. The given reaction enthalpies were calculated from the enthalpies of formation of neutrals<sup>1</sup> and electron affinities.<sup>2,3</sup> The formation of metastable  $H_2O^-$  via radiative association is also energetically allowed,<sup>4</sup> but this process has not yet been confirmed experimentally. Studying the temperature dependence of the two reactions provides a probe for investigating the structure and reactivity of the fundamental  $H_2O^-$  system at low energies. At higher energies, this system has recently been studied theoretically<sup>5</sup> and experimentally<sup>6–8</sup> by means of dissociative electron attachment to the neutral water molecule. Other studies include the work of Claydon *et al.*<sup>9</sup> and the detailed potential energy surface calculations of Werner *et al.*<sup>4</sup>

Experimental studies of the rate coefficients of reactions (1) and (2) and their temperature dependencies have been carried out before at room temperature and above using drift tubes, flowing afterglow, tandem mass spectrometry, and an octopole ion trap instrument.<sup>10,11</sup> A study at mean collision

energies down to 0.02 eV was carried out using a temperature variable flow/drift tube.<sup>12</sup> Furthermore, the kinetic energy distribution of the electrons produced in associative detachment has been studied by Mauer and Schulz,<sup>13</sup> Esaulov *et al.*,<sup>14</sup> and Jusko *et al.*<sup>11</sup> Using crossed beams, energy partitioning in the  $O^- + D_2 \rightarrow OD^- + D$  reaction has been reported recently by Lee and Farrar.<sup>15</sup> The results of all these studies indicate high internal excitation of the produced  $H_2O$  neutrals and slow electrons. For further details and references see Ref. 11.

When  $O^-(^2P)$  approaches  $H_2(X^1\Sigma_g^+)$ , the collision system can follow three electronic surfaces which can be marked according to their corresponding irreducible representations as  $1^2A'$ ,  $1^2A''$ , and  $2^2A'$ . Furthermore, the  $O^-$  ion can be present in two fine structure states,  $O^-(^2P_{3/2})$  and  $O^-(^2P_{1/2})$ , which is 22 meV higher.<sup>16</sup> Molecular hydrogen is present in two nuclear spin configurations: *ortho*- and *para*- $H_2$ . The lowest rotational states of *ortho*- and *para*- $H_2$  are separated by  $\approx 15$  meV. In the present experiments, we are using normal hydrogen; hence, the ratio of *ortho*-/*para*- $H_2$  concentrations is fixed at the statistical value, 3:1 (see discussion in Ref. 17). Concerning the population of the two  $O^-$  fine structure states, reached in the trap via collisions with He and  $H_2$ , we can only speculate. Analysis of drift tube experiments by Viehland *et al.*<sup>18</sup> suggests that the relaxation of fine structure states of  $O^-$  by collisions with helium is slow and the ratio of  $O^-(^2P_{1/2})$  to  $O^-(^2P_{3/2})$  concentration is 1:2 according to the statistical probability of production in the ion source. Collisions with  $H_2$  are not expected to contribute to relaxation, because at low temperatures almost every collision of  $O^-$  with  $H_2$  is reactive.

This work presents an experimental and theoretical study of collisions of  $O^-$  with  $H_2$  at low temperatures. In the following, we will first describe the experiment and the measured temperature dependencies of rate coefficients for AD and hydrogen atom transfer. In the section Calculations and

<sup>a)</sup>Author to whom correspondence should be addressed. Electronic mail: [Stepan.Roucka@mff.cuni.cz](mailto:Stepan.Roucka@mff.cuni.cz)

theory, we introduce briefly into the calculation of the  $\text{H}_2\text{O}^-$  potential energy surfaces and provide a detailed basis for explaining the measured results. In Conclusions, we summarize the results and provide some information on planned work.

## II. EXPERIMENT

To study reactive collisions of  $\text{O}^-$  ions with  $\text{H}_2$ , we used the cryogenic 22-pole radiofrequency ion trap. Because a thorough description of the instrument can be found elsewhere,<sup>19–21</sup> only a few hints are given here. Primary  $\text{O}^-$  ions are produced by electron bombardment of  $\text{N}_2\text{O}$  precursor gas in a storage ion source.<sup>22</sup> The ions are extracted from the ion source, mass selected, and injected into the linear 22-pole radiofrequency ion trap.<sup>22,23</sup> The trap is cooled by a cryocooler reaching temperatures down to 10 K. The injected ions are thermalized to the trap temperature by collisions with helium buffer gas. The number density of helium is typically 100 times higher than the number density of the  $\text{H}_2$  reactant gas, which is also leaked into the trap. The absolute number density of the reactant, which is required for determination of absolute rate coefficients, is determined using a Bayard-Alpert ionization gauge. A standard procedure for calibrating the ionization gauge using a spinning rotor gauge is used. We estimate that the total systematic error of the number density is below 20%. After a certain trapping/reaction time, the ions are extracted from the trap, mass selected, and counted using a microchannel plate detector. By repeating this procedure for different selected masses, trapping times, and  $\text{H}_2$  densities, one can obtain the time evolution of relative numbers of ions in the trap. In particular, the relative numbers of  $\text{O}^-$  and  $\text{OH}^-$  ions, denoted by  $N_{\text{O}}$  and  $N_{\text{OH}}$ , respectively, were measured for several  $\text{H}_2$  densities as a function of time after injection of  $\text{O}^-$  ions to the trap.

## III. EXPERIMENTAL RESULTS

A typical measured time evolution of the numbers of trapped primary  $\text{O}^-$  and product  $\text{OH}^-$  ions,  $N_{\text{O}}$  and  $N_{\text{OH}}$ , is shown in Fig. 1, at various trap temperatures. The measurements were performed at constant  $\text{H}_2$  flux resulting in different hydrogen densities at different temperatures. In order to make the results comparable, we show how the data would appear if the  $[\text{H}_2]$  were equal  $10^{10} \text{ cm}^{-3}$  in each measurement. This is achieved by using a reduced trapping time  $t^\# = t \times [\text{H}_2] / (10^{10} \text{ cm}^{-3})$ . In this way, the slopes of the  $\text{O}^-$  number decays are proportional to the reaction rate coefficients at the respective temperatures. Since the  $\text{H}_2$  flux was not adjusted between the presented measurements, the relative values are not affected by the systematic uncertainty of  $[\text{H}_2]$ .

The data were analyzed by least-squares fitting the measured numbers of ions with the analytic solutions of the corresponding kinetic equations. The good agreement of the fit with the measured data is illustrated in Fig. 1. At temperatures above 200 K, we observed a loss of  $\text{O}^-$  ions even without adding  $\text{H}_2$ . One of the reasons is the  $\text{N}_2\text{O}$  gas from the ion source, which is efficiently cryopumped at lower temperatures. In such cases, the loss rate is measured separately for the

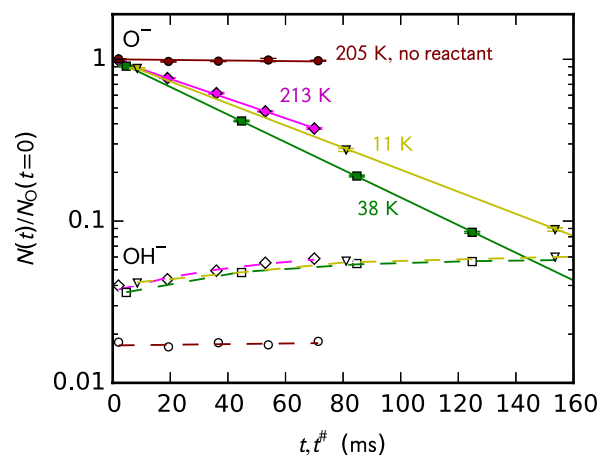


FIG. 1. Decay of the number of primary  $\text{O}^-$  ions and increase of the number of  $\text{OH}^-$  product ions due to interaction of  $\text{O}^-$  ions with  $\text{H}_2$ . The data were measured at several trap temperatures (indicated in the graph). The numbers of  $\text{O}^-$  and  $\text{OH}^-$  ions relative to the initial number of  $\text{O}^-$  ions are indicated by full and empty symbols, respectively. The number density of  $\text{H}_2$  at 213 K was  $1.0 \times 10^{10} \text{ cm}^{-3}$ . The data at 11 K and 38 K are plotted as a function of reduced trapping time  $t^\#$ , accounting for the change of density with temperature at constant gas flux (see text). The fitted curves are indicated by lines. The data measured at 205 K without  $\text{H}_2$  reactant present are shown for comparison.

given temperature and it is included in our analysis. Also for  $\text{OH}^-$  ions, an additional loss was observed at temperatures above 200 K and included in the kinetic equations as an additional term. This increased the uncertainty of the fitted values of  $k_2$ ; hence, more datasets had to be averaged in order to reach the desired accuracy at 300 K. At temperatures below 200 K, the  $\text{OH}^-$  loss is negligible as verified by repeating the analysis with the  $\text{OH}^-$  loss process included.

From the evaluated time dependencies and the known number densities of  $\text{H}_2$ , the reaction rate coefficients for both reaction channels were calculated. Measured linear dependencies of the loss rate on  $[\text{H}_2]$  confirmed that the evaluated rate coefficients correspond to a binary reaction with  $\text{H}_2$ . By varying the trap temperature, the rate coefficients of both reactions were measured in the temperature range of 10–300 K. For reaction (2), the accuracy of measurements at temperatures above 200 K is limited due to parasitic reactions. In order to test the influence of desorbing impurities, measurements were performed during the cooling down phase as well as the warming up phase (cold head switched off). As can be seen from Fig. 2, there are no significant differences in the results. The rate coefficient of reaction (1) has a flat maximum of about  $1.8 \times 10^{-9} \text{ cm}^3 \text{ s}^{-1}$  in the temperature range of 20–80 K, which exceeds the Langevin rate coefficient  $k_{\text{Lang}} = 1.56 \times 10^{-9} \text{ cm}^3 \text{ s}^{-1}$  (the polarizability of normal- $\text{H}_2$  at 77 K was used to calculate  $k_{\text{Lang}}$ ,<sup>24</sup> neglecting the small temperature dependence). Similar temperature dependence was recently observed for reaction of  $\text{NH}_2^-$  with  $\text{H}_2$ .<sup>25</sup> Reaction (2) proceeds with a nearly constant rate coefficient of  $5 \times 10^{-11} \text{ cm}^3 \text{ s}^{-1}$  corresponding to a reaction probability of approximately  $k_2/k_{\text{Lang}} \approx 0.03$ . The slight decrease down to 10 K may indicate an increase of adiabatic behavior at these low velocities.

For comparison, Fig. 2 also shows a collection of results obtained in previous studies (see figure caption). The value

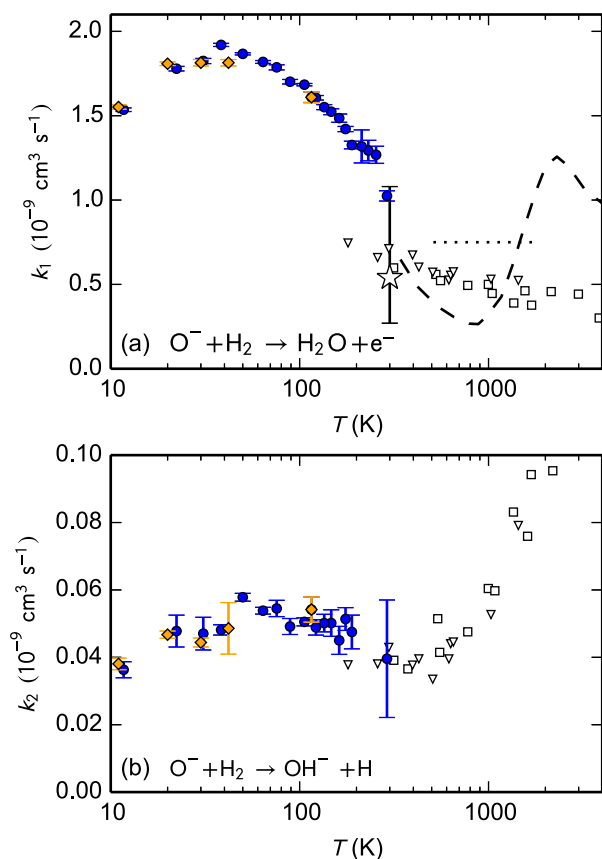


FIG. 2. Temperature dependence of the rate coefficients for associative detachment (panel (a)) and H atom transfer reactions (panel (b)). The data measured in the present experiments are indicated by the filled symbols (diamonds: warming up phase and circles: cooling down phase). The error bars indicate only the statistical errors of the fits. The overall uncertainty of the absolute values is  $\pm 20\%$ . The hollow star indicates data measured recently using an octopole ion trap at 300 K in our laboratory.<sup>11</sup> The figures also show various results measured with drift tubes: hollow squares: McFarland *et al.*,<sup>10</sup> triangles: Viggiano *et al.*,<sup>12</sup> and dotted lines: Moruzzi *et al.*<sup>26</sup> The dashed line shows ion beam data<sup>13</sup> reported by McFarland *et al.*<sup>10</sup>

marked by a hollow star in panel (a) of Fig. 2 was measured in an octopole radiofrequency ion trap at 300 K by detecting the electrons produced in AD (reaction (1)).<sup>11</sup> This result is accurate within a factor of 2 due to systematic errors. Note that the primary goal of those studies was to record the energy distribution of electrons produced in AD.

Inspection of the overall temperature dependence of the rate coefficients indicates interesting trends. Note, however, that our results are thermal rate coefficients at temperatures  $\leq 300 \text{ K}$  while drift tube data were obtained at mean collision energies  $\text{KE}_{\text{CM}}$ . They are plotted at corresponding temperatures above 300 K (with exception of one value at 176 K<sup>12</sup>). The rate coefficient of reaction (2) is certainly a continuous extension of the data by McFarland *et al.*<sup>10</sup> and Viggiano *et al.*<sup>12</sup> while the rate coefficients of reaction (1) show a step at 300 K. However, considering that the overall uncertainty of our data is 20%, and the systematic and statistical errors of Viggiano *et al.*<sup>12</sup> are 25% and 15%, respectively, this step is nearly insignificant. It may be caused partly due to parasitic reactions in the trap at temperatures above 200 K but also due to errors in the older experiments. Nonetheless, there is

no doubt that the overall reactivity of  $\text{O}^-$  and  $\text{H}_2$  increases steeply with temperature decreasing below 300 K. In the following, we provide a tentative explanation based on non-adiabatic coupling of the repulsive potential energy surfaces to the reactive one.

#### IV. CALCULATIONS AND THEORY

The complete theoretical description of the reactive  $\text{O}^- + \text{H}_2$  scattering is beyond the scope of this article and it will be subject of a subsequent paper. Here, we present some preliminary calculations and qualitative reasoning giving some insight into the dynamics of the processes of the interest. This section is organized as follows. We present the details of the *ab initio* calculation in Subsection IV A. The cuts of the lowest three potential energy surfaces (PES) along the reactive coordinate are also discussed there. These cuts indicate that only one of the three PES contributes to AD reaction. Finally, we discuss briefly the global topology of these surfaces including the information about the conical intersection structure. In Subsection IV B, we argue that the conical intersection is responsible for the fact that all three surfaces finally contribute to the process (as suggested by the size of the measured rate exceeding the Langevin rate). This argument is supported by classical trajectory calculations that are limited to individual uncoupled surfaces (calculation of the nonadiabatic coupling of the surfaces is left for the subsequent work). No quantitative information on reaction cross sections and branching ratios can be given as long as we neglect the nonadiabatic coupling. We thus remain on the qualitative level of discussion there. In Subsection IV C, a simplified quantitative model is, nevertheless, developed for the capture cross section. We believe that this model is relevant for explaining the shallow maximum in measured rates near 40 K.

##### A. *Ab initio* potential energy surfaces

First, we have calculated the potential energy surfaces for the three lowest electronic states leading to the  $\text{O}^-(^2\text{P}) + \text{H}_2(\text{X}^1\Sigma_g^+)$  asymptote ( $1^2\text{A}'$ ,  $1^2\text{A}''$ , and  $2^2\text{A}$ ). The positions of the nuclei were parameterized with Jacobi coordinates  $R$  (distance between nucleus of O and the center of mass of  $\text{H}_2$ ),  $r$  (mutual distance of the two H atoms), and  $\theta$  (angle between  $R$  and  $r$  vectors). Calculations have been done with the MOLPRO package<sup>27,28</sup> using the internally contracted multireference configuration interaction (MRCI) method<sup>29</sup> starting from MCSCF<sup>30,31</sup> with 1 closed orbital and 9 electrons in 10 active orbitals. In order to obtain the best results possible today, we did all calculations with aug-cc-pVTZ.<sup>32</sup> To localize the two-dimensional surface, where the anion states are embedded in the electron continuum, also the lowest state of the neutral  $\text{H}_2\text{O}$  molecule has been determined on the same level of theory. The potential energy surfaces were obtained on a fine grid with  $\theta \in \langle 0^\circ, 90^\circ \rangle$  with step  $10^\circ$ ,  $R \in \langle 2a_0, 10a_0 \rangle$  and  $\langle 10a_0, 20a_0 \rangle$  with steps  $0.2a_0$  and  $0.5a_0$ , respectively, and  $r \in \langle 1.0a_0, 2.0a_0 \rangle$  and  $\langle 2.0a_0, 2.9a_0 \rangle$  with steps  $0.05a_0$  and  $0.1a_0$ , respectively. All distances here and in the rest of the

paper are given in atomic units (Bohr radius  $a_0$ ). As compared to previous calculation of Werner *et al.*,<sup>4</sup> our active space is bigger and we used all configurations from the active space as reference wave functions in MRCI calculations. Although our MRCI results include more electron correlation than those of Werner *et al.*,<sup>4</sup> the asymptotic energy difference between  $O^- + H_2$  and  $OH^- + H$  channels by 0.1 eV is too small as compared to the experimental value of 0.28 eV. To improve the asymptotic behavior of the PES, we used the Davidson correction as implemented in MOLPRO<sup>33</sup> for which the energy difference is 0.23 eV.

To visualize the PES relevant for the understanding reactions (1) and (2), Fig. 3 shows one-dimensional cuts of PES along two paths connecting  $O^- + H_2$  and  $OH^- + H$  asymptotic regions. In panel (a), the adiabatic potential energy for all three ( $1^2A'$ ,  $1^2A''$ , and  $2^2A'$ ) states is plotted along the reaction coordinate (minimum energy path), together with the potential energy of the neutral molecule  $H_2O$ . The autodetachment can occur in the region where the anionic curve is above the neutral (this region is responsible for  $e^- + H_2O$  product channel). Strictly speaking, the electron-molecule scattering

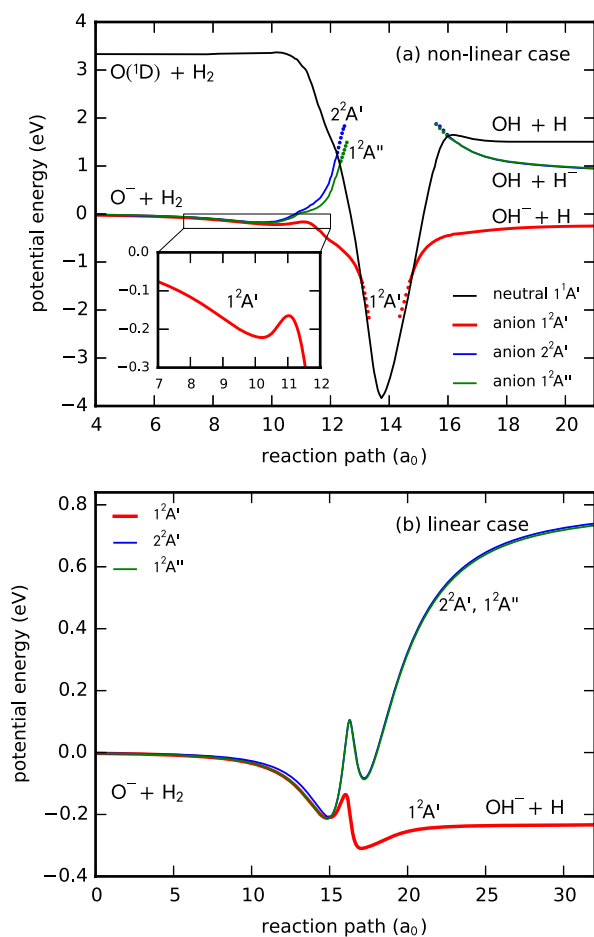


FIG. 3. Panel (a)—PES of  $H_2O^-$  and  $H_2O$  along the minimum energy path going from  $O^- + H_2$  to  $OH^- + H$  on the  $1^2A'$  PES. The anionic curves in the autodetachment region, where they are above the neutral PES, are indicated by points. The local minimum of the  $1^2A'$  PES, where some metastable  $H_2O^-$  states may exist, is magnified in the inset. In panel (b), the path is constrained to the linear geometry,  $\theta = 0^\circ$ . In this case, the potential energy of the neutral  $H_2O$  is too high—outside of the graph.

calculation must be used to continue the curves deep into this region. We thus show only short portion of the PES calculated from quantum chemistry with the dashed lines. In panel (b), the minimum energy path is restricted to a linear molecular geometry (similar potential curve was shown for older calculation by Werner *et al.*<sup>4</sup>). Here, the neutral  $H_2O$  PES cannot be shown because it is far up, out of the energy scale of the graph. Inspection of the upper panel reveals that the system following the minimum energy path on the ground  $1^2A'$  PES passes through the autodetachment region, while the PES of the other two states are repulsive and do not allow to reach this region in low-energy collisions directly. There are also trajectories possible (e.g., along the linear PES shown in (b)) where the autodetachment region is avoided and one may reach the  $OH^- + H$  product channel without electron detachment. However, it is energetically preferable to bend the molecule and to follow the path shown in Fig. 3(a). This, together with a high probability of autodetachment, provides a first qualitative explanation for the small  $k_2$  observed in the experiment.

More qualitative insight into the collision dynamics can be gained by inspecting the three surfaces that the  $O^- + H_2$  system has to follow during the first approach. In statistical theories, it is common to account for repulsive surfaces with a weighting factor which would be here 1/3 if the surfaces are not coupled at all. However, this does not apply to the present anionic system, because all three PES are first attractive before they split. This situation is shown in more detail in Fig. 4(a). The data in this figure are calculated in linear geometry (with  $\theta = 0^\circ$ ,  $r = 1.4a_0$ ) since the minimum energy path follows this line down to an  $O^- - H_2$  distance of  $4.5a_0$ . Note that two of the three states are degenerate, forming a  $2^2\Pi$  state due to the additional symmetry in linear geometry. All three PES follow the asymptotic behavior within  $\sim 10$  meV. We can therefore expect that first capture at low collision energies can be rather well understood from the motion in a potential that is close to the average of the three PES. Another important feature seen in Fig. 4(a) (see also the inset) is the conical intersection near  $R = 4.6a_0$ , which couples all three states in the vicinity of the local potential minimum. To understand the global geometry of the conical intersection, we have to keep in mind that two of the PES are degenerate at linear geometry (it is  $1^2A'$  and  $1^2A''$  for  $R$  larger than the intersection point and  $2^2A'$  and  $1^2A''$  for small  $R$ ). The three PES are thus just the three branches of one 3-dimensional self-intersecting surface, which intersects itself at linear geometry (2-dimensional intersection) and at a 1-dimensional curve ( $R = 4.6a_0$ ,  $\theta = 0^\circ$ ,  $r = 1.4a_0$  is one representative point of this triple intersection). It is beyond the scope of the present paper to describe the nonadiabatic dynamics on this PES manifold and how and where the electron is ejected. Autoionization widths and the coefficients for nonadiabatic and spin-orbit coupling have to be found first. However, we will try to learn from the classical trajectory calculations on the three PES, disregarding any coupling.

## B. Classical trajectories on uncoupled PES

First, we followed a set of trajectories on the lowest PES. All trajectories start in the asymptotic region  $R \rightarrow \infty$  with the hydrogen molecule close to its equilibrium geometry  $r = 1.4a_0$

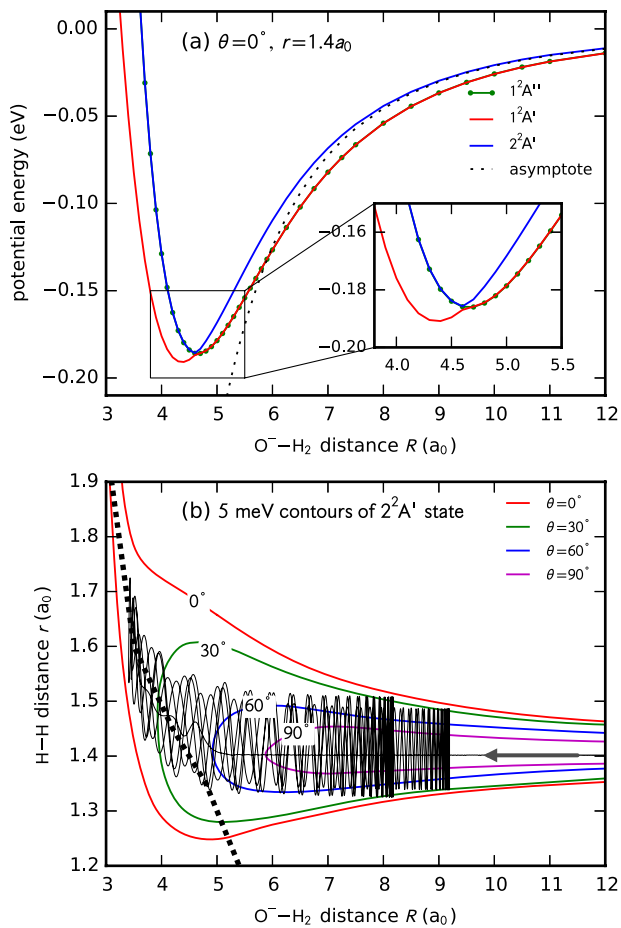


FIG. 4. Panel (a)—Section of the three potential energy surfaces for  $\theta = 0^\circ$ ,  $r = 1.4014a_0$ , showing the attraction of  $O^-$  and  $H_2$  and the conical intersection at  $4.6a_0$ , coupling them. The sum of quadrupole and polarization potential is marked with a dotted line. Panel (b)—Typical classical trajectory on the  $2^2A'$  PES for a collision energy of 5 meV projected on the  $\theta = 0^\circ$  plane. The conical intersection at  $\theta = 0^\circ$  is marked by the dashed line. The equipotential lines for  $V = 5$  meV are also shown for the indicated values of  $\theta$ . This picture shows a section of a trajectory with a duration of 700 vibrational periods of  $H_2$ . Most trajectories remain trapped for typically  $10^4$ – $10^5$  vibrational periods, passing beyond the conical intersection several hundred times.

and with arbitrary initial orientation  $\theta$ . The behavior of typical trajectories is as follows. As the colliding particles approach each other, the molecule has a tendency to align ( $\theta \rightarrow 0^\circ$ ) due to the long range quadrupole potential, staying close to reaction path (Fig. 3(a)). When reaching the interaction region  $R \approx 3a_0$  on the PES of the ground state  $1^2A'$ , the trajectory is deflected towards the  $OH^- + H$  asymptote by stretching  $r$ . The angle  $\theta$  increases at the same time. When moving on the  $1^2A'$  ground electronic PES the trajectory can continue to the autodetachment region at  $r \approx 2.2a_0$  and  $\theta \approx 60^\circ$ . For treating electron detachment, the autodetachment mechanism must be quantified (autodetachment width). The measured energy distribution of electrons<sup>11</sup> suggests that the detachment is efficient, as it occurs soon after crossing the PES of the neutral. Also the measured rate coefficient of associative detachment between  $OH^-$  and H shows that nearly every collision leads to detachment.<sup>34</sup> We also expect, in accordance with Fig. 3(b) that some trajectories can reach the  $OH^- + H$  exit channel, avoiding

the detachment region. According to the experimental results, this process occurs with small probability.

As shown already in Fig. 3(a), trajectories on the upper two electronic states cannot lead directly to autodetachment or rearrangement at low collision energies. A typical trajectory for the  $2^2A'$  PES and the position of the conical intersection among the three electronic states at  $\theta = 0^\circ$  (black dashed line) are shown in Fig. 4(b). The starting point of the trajectory is at the right ( $R = 12a_0$  and  $r = 1.4a_0$ ) and the particles are approaching each other on a straight line. During the reflection at short distances, vibration along the coordinate  $r$  is excited. The conversion of translational energy into vibration of  $H_2$  hinders or forbids dissociation back to the initial channel. The trajectory thus becomes trapped in a long lived collision complex. It is easy to see that it passes beyond the conical intersection many times. Strictly speaking, the trajectory on single PES does not make sense beyond the conical intersection point since the  $2^2A'$  becomes degenerate with  $1^2A''$  each time the system passes through the linear geometry enhancing the nonadiabatic coupling among PES. This corroborates our speculation from above: the many attempts accumulate to a large probability to jump to the lowest  $1^2A'$  state from where it does not come back because it can continue its way towards the autodetachment region or to the H atom transfer channel. It is thus plausible to assume that all three PES contribute to the detachment cross section (the lowest one directly and upper two through the conical intersection). We have already stressed that we cannot give more quantitative statement about the branching into individual product channels without accounting for nonadiabatic coupling, but in Subsection IV C we try to quantify the capture cross section for the formation of just described long lived collision complex.

### C. Model for low-energy capture rate

Qualitative discussion in Subsections IV A and IV B suggests, that at low enough energies, the sum of the AD (the dominant channel) and the H atom transfer rate coefficients will become close to the total capture rate coefficient. To explain qualitatively the behavior of the rate coefficient at very low energies (where experiment shows deviations from the Langevin rate), we performed calculation of the cross section of capture within a simple 1D model with the following effective 1D potential model (in hartrees):

$$\frac{V(R/a_0)}{\text{Ha}} = -\frac{2.74}{R^4} + 0.0015(e^{-1.4(R-5.5)} - 2e^{-0.7(R-5.5)}). \quad (3)$$

This function is obtained from *ab initio* data for  $R > 3a_0$ . To take into account possibility of reorientation and stretching of the molecule, we take the *ab initio* data at fixed- $R$  and diagonalize the Hamiltonian in  $r, \theta$  space. The  $R$ -dependence of the lowest eigenvalue then produces the one dimensional potential energy curve for each of the three PES. Finally, the function  $V(R)$  above is the least squares fit to the average of the three thus obtained curves.  $V(R)$  is replaced by a constant for  $R < 3a_0$ , since this region is not important for capture at low energies. Furthermore, at small  $R$ , we include the complex

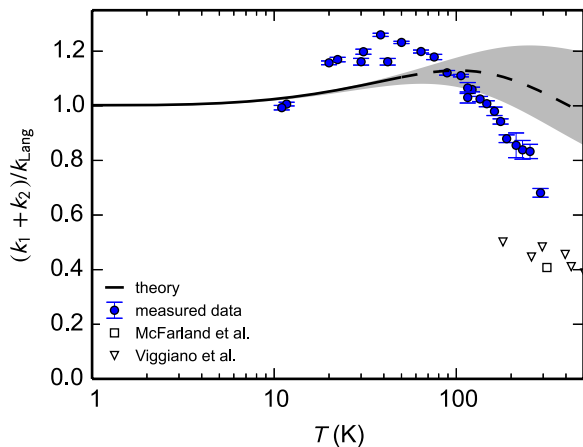


FIG. 5. Comparison of the measured total reaction rate coefficients  $k_1 + k_2$  with the values calculated with the 1D capture model described in the text. The data are normalized with the Langevin capture rate coefficient. Sensitivity test of the model is indicated with the gray area. The part of the theoretical curve which is significantly sensitive to the parameters of the absorbing potential, is shown as a dashed line. Experimental results of McFarland *et al.*<sup>10</sup> and Viggiano *et al.*<sup>12</sup> are shown for comparison.

absorbing potential equal to  $-i/2 \times \Gamma(R)$ , with

$$\frac{\Gamma(R/a_0)}{\text{Ha}} = A[1 + e^{5(R-R_c)}] - 1. \quad (4)$$

The total absorption cross section for this potential is calculated solving the radial Schrödinger equation for sufficient number of partial waves. The cross section is integrated over Maxwell-Boltzmann collision energy distribution. The resulting capture rate coefficient is shown in Fig. 5, together with our experimental data for AD. We also show the uncertainty of the capture model due to the absorbing function  $\Gamma(R)$  by varying the strength  $A$  between 0.2 and 1.0 and the position  $R_c$  between  $2.5a_0$  and  $3.5a_0$ . To emphasize the small deviations from the simple Langevin model, we show in Fig. 5 the rate coefficient of reaction (1) normalized to the Langevin capture rate coefficient.

The calculated rate coefficient qualitatively agrees with the measured curve. Its size even slightly exceeds the Langevin value due to additional short range attractive term somewhat strengthening the polarization potential. The presence of the maximum (and the associated drop in rate towards the lowest temperatures) can thus be directly related to the shape of the potential. The exact position of the maximum does not match the observed data. We attribute this mismatch to the averaging procedure used to produce the capture model. For more precise capture coefficient, we need to take into account the nonadiabatic coupling and not just the average, since two of the three PES are degenerate in linear geometry for each value of  $R$ . The calculated data also show the decrease of the rate at higher temperature but we expect that the simple capture model is not correct at higher end of temperature axis in Fig. 5.

## V. CONCLUSIONS AND OUTLOOK

The rate coefficients of associative detachment and hydrogen atom transfer between  $\text{O}^-$  and  $\text{H}_2$  have been measured

at temperatures between 10 K and 300 K. This work thus provides data at so far unexplored temperatures below 176 K. The rate coefficient of associative detachment increases with decreasing temperature between 300 K and 80 K, then levels off at  $1.8 \times 10^{-9} \text{ cm}^3 \text{ s}^{-1}$  between 80 K and 20 K, and finally decreases again to the value of  $1.5 \times 10^{-9} \text{ cm}^3 \text{ s}^{-1}$  at 10 K. The rate coefficient of hydrogen atom transfer has a nearly constant value of  $5 \times 10^{-11} \text{ cm}^3 \text{ s}^{-1}$  with a slight decrease at 10 K. The unexpectedly high value of the associative detachment rate coefficient is explained with the aid of calculated PES of  $\text{H}_2\text{O}^-$ . The classical trajectory simulations suggest that a long-lived complex is formed in collisions on the attractive PES at low collision energies and that there is a high probability of transition to the reactive PES due to the conical intersection, which means that the reaction rate coefficient will be close to the capture rate coefficient. Since all three potentials are following closely the quadrupole + polarization behavior at large  $\text{O}^- + \text{H}_2$  separation, this capture rate is close to Langevin rate at low temperature. The Langevin value is even little bit exceeded (in accordance with measured data) since the PES are even slightly more attractive than the quadrupole + polarization. With increasing collision energy, the lifetime of the collision complex decreases due to easier possibility to escape back through attractive potential energy well and the rate coefficient approaches the fraction of Langevin rate. Furthermore, the presence of long-lived  $\text{H}_2\text{O}^-$  complexes points to the possibility of ternary association, i.e., stabilization by collision with third particle and consequent formation of metastable  $\text{H}_2\text{O}^-$ . Experimentally determined branching ratios show that hydrogen atom transfer occurs in less than 5% of reactive collisions. This observation can be explained by noticing that the reaction path of hydrogen atom transfer passes through autodetachment region. The paths that avoid autodetachment have to balance on the higher potential energy shelf, which is less probable.

The observed data are thus in good agreement with the theoretical arguments that follow from the calculated PES. However, to get a deeper understanding, further experimental and theoretical studies are needed. Experimental study of the isotopic effect of exchanging  $\text{H}_2$  for  $\text{D}_2$  is in preparation and we are planning to study the differences in reactivity between *ortho* and *para* nuclear spin configurations of  $\text{H}_2$  by means of the 22-pole trap combined with a para-hydrogen generator.

We also plan to deepen our theoretical understanding of the dynamics in several respects. First, we will determine the autodetachment widths by running the  $R$ -matrix calculation<sup>35,36</sup> of electron scattering on water molecule with relevant geometries. From this calculation, we plan to construct the nonlocal resonance model for the associative detachment, as we did previously for several diatomic systems.<sup>37–39</sup> Finally, we will also calculate the nonadiabatic and spin-orbit coupling among the three anionic states and run the scattering calculation of the nuclear dynamics to get state to state cross sections for both reactions (1) and (2).

## ACKNOWLEDGMENTS

We thank the Technische Universität Chemnitz and the Deutsche Forschungsgemeinschaft for lending the 22-pole trap

instrument to the Charles University. This work was partly supported by the Czech Grant Agency (GACR P209/12/0233, GACR 14-14715P, GACR 208/10/1281) and by the Charles University (UNCE 204020/2012, GAUK 659112).

- <sup>1</sup>M. W. Chase and National Institute of Standards and Technology (U.S.), *NIST-JANAF Thermochemical Tables* (American Chemical Society, Woodbury, NY; American Institute of Physics for the National Institute of Standards and Technology, Washington, DC, 1998).
- <sup>2</sup>J. R. Smith, J. B. Kim, and W. C. Lineberger, *Phys. Rev. A* **55**, 2036 (1997).
- <sup>3</sup>C. Blondel, W. Chaibi, C. Delsart, C. Drag, F. Goldfarb, and S. Kröger, *Eur. Phys. J. D* **33**, 335 (2005).
- <sup>4</sup>H. J. Werner, U. Manz, and P. Rosmus, *J. Chem. Phys.* **87**, 2913 (1987).
- <sup>5</sup>D. J. Haxton, C. W. McCurdy, and T. N. Rescigno, *Phys. Rev. A* **75**, 012710 (2007).
- <sup>6</sup>H. Adaniya, B. Rudek, T. Osipov, D. J. Haxton, T. Weber, T. N. Rescigno, C. W. McCurdy, and A. Belkacem, *Phys. Rev. Lett.* **103**, 233201 (2009).
- <sup>7</sup>D. J. Haxton, H. Adaniya, D. S. Slaughter, B. Rudek, T. Osipov, T. Weber, T. N. Rescigno, C. W. McCurdy, and A. Belkacem, *Phys. Rev. A* **84**, 030701(R) (2011).
- <sup>8</sup>N. B. Ram, V. S. Prabhudesai, and E. Krishnakumar, *J. Phys. B: At. Mol. Opt. Phys.* **42**, 225203 (2009).
- <sup>9</sup>C. R. Claydon, G. A. Segal, and H. S. Taylor, *J. Chem. Phys.* **54**, 3799 (1971).
- <sup>10</sup>M. McFarland, D. L. Albritton, F. C. Fehsenfeld, E. E. Ferguson, and A. L. Schmeltekopf, *J. Chem. Phys.* **59**, 6629 (1973).
- <sup>11</sup>P. Jusko, Š. Roučka, R. Plašil, and J. Glosík, *Int. J. Mass Spectrom.* **352**, 19 (2013).
- <sup>12</sup>A. A. Viggiano, R. A. Morris, C. A. Deakyne, F. Dale, and J. F. Paulson, *J. Phys. Chem.* **95**, 3644 (1991).
- <sup>13</sup>J. L. Mauer and G. J. Schulz, *Phys. Rev. A* **7**, 593 (1973).
- <sup>14</sup>V. A. Esaulov, R. L. Champion, J. P. Grouard, R. I. Hall, J. L. Montmagnon, and F. Penent, *J. Chem. Phys.* **92**, 2305 (1990).
- <sup>15</sup>S. T. Lee and J. M. Farrar, *J. Chem. Phys.* **111**, 7348 (1999).
- <sup>16</sup>C. Blondel, C. Delsart, C. Valli, S. Yiou, M. R. Godefroid, and S. Van Eck, *Phys. Rev. A* **64**, 052504 (2001).
- <sup>17</sup>I. Zymak, M. Hejduk, D. Mulin, R. Plašil, J. Glosík, and D. Gerlich, *Astrophys. J.* **768**, 86 (2013).
- <sup>18</sup>L. A. Viehland, R. Webb, E. P. Lee, and T. G. Wright, *J. Chem. Phys.* **122** (2005).
- <sup>19</sup>D. Gerlich, G. Borodi, A. Luca, C. Mogo, and M. A. Smith, *Z. Phys. Chem.* **225**, 475 (2011).
- <sup>20</sup>I. Zymak, P. Jusko, Š. Roučka, R. Plašil, P. Rubovič, D. Gerlich, and J. Glosík, *Eur. Phys. J. Appl. Phys.* **56**, 24010 (2011).
- <sup>21</sup>D. Gerlich, P. Jusko, Š. Roučka, I. Zymak, R. Plašil, and J. Glosík, *Astrophys. J.* **749**, 22 (2012).
- <sup>22</sup>D. Gerlich, *Adv. Chem. Phys.* **82** (1992).
- <sup>23</sup>D. Gerlich, *Phys. Scr.* **1995**, 256.
- <sup>24</sup>Y. Y. Milenko, L. V. Karnatsevich, and V. S. Kogan, *Physica* **60**, 90 (1972).
- <sup>25</sup>R. Otto, J. Mikosch, S. Trippel, M. Weidemüller, and R. Wester, *Phys. Rev. Lett.* **101**, 063201 (2008).
- <sup>26</sup>J. L. Moruzzi, J. J. W. Ekin, and A. V. Phelps, *J. Chem. Phys.* **48**, 3070 (1968).
- <sup>27</sup>H.-J. Werner, P. J. Knowles, G. Knizia, F. R. Manby, and M. Schütz, *Wiley Interdiscip. Rev.: Comput. Mol. Sci.* **2**, 242 (2012).
- <sup>28</sup>H.-J. Werner, P. J. Knowles, G. Knizia, F. R. Manby, M. Schütz, P. Celani, T. Korona, R. Lindh, A. Mitrushenkov, G. Rauhut, K. R. Shamasundar, T. B. Adler, R. D. Amos, A. Bernhardsson, A. Berning, D. L. Cooper, M. J. O. Deegan, A. J. Dobbyn, F. Eckert, E. Goll, C. Hampel, A. Hesselmann, G. Hetzer, T. Hrenar, G. Jansen, C. Köppl, Y. Liu, A. W. Lloyd, R. A. Mata, A. J. May, S. J. McNicholas, W. Meyer, M. E. Mura, A. Nicklass, D. P. O'Neill, P. Palmieri, D. Peng, K. Pflüger, R. Pitzer, M. Reiher, T. Shiozaki, H. Stoll, A. J. Stone, R. Tarroni, T. Thorsteinsson, and M. Wang, *MOLPRO, Version 2012.1, A Package of Ab Initio Programs* (University College Cardiff Consultants Limited, Cardiff, UK, 2012).
- <sup>29</sup>P. Knowles and H.-J. Werner, *Theor. Chim. Acta* **84**, 95 (1992).
- <sup>30</sup>H.-J. Werner and P. J. Knowles, *J. Chem. Phys.* **82**, 5053 (1985).
- <sup>31</sup>P. J. Knowles and H.-J. Werner, *Chem. Phys. Lett.* **115**, 259 (1985).
- <sup>32</sup>T. H. Dunning, *J. Chem. Phys.* **90**, 1007 (1989).
- <sup>33</sup>H.-J. Werner, M. Kállay, and J. Gauss, *J. Chem. Phys.* **128**, 034305 (2008).
- <sup>34</sup>C. J. Howard, F. C. Fehsenfeld, and M. McFarland, *J. Chem. Phys.* **60**, 5086 (1974).
- <sup>35</sup>J. Tennyson, *Phys. Rep.* **491**, 29 (2010).
- <sup>36</sup>J. M. Carr, P. G. Galiatsatos, J. D. Gorfinkiel, A. G. Harvey, M. A. Lysaght, D. Madden, Z. Mašín, M. Plummer, J. Tennyson, and H. N. Varambhia, *Eur. Phys. J. D* **66**, 58 (2012).
- <sup>37</sup>M. Čížek, J. Horáček, and W. Domcke, *J. Phys. B: At. Mol. Opt. Phys.* **31**, 2571 (1998).
- <sup>38</sup>K. Houfek, M. Čížek, and J. Horáček, *Phys. Rev. A* **66**, 062702 (2002).
- <sup>39</sup>S. Živanov, M. Allan, M. Čížek, J. Horáček, F. A. U. Thiel, and H. Hotop, *Phys. Rev. Lett.* **89**, 073201 (2002).